Journal of Materials Chemistry A

PAPER

View Article Online
View Journal | View Issue

Cite this: J. Mater. Chem. A, 2014, 2, 5703

Bidentate-complex-derived TiO_2/carbon dot photocatalysts: *in situ* synthesis, versatile heterostructures, and enhanced H_2 evolution†

Jing Wang, Minmin Gao and Ghim Wei Ho*

Received 10th December 2013
Accepted 3rd February 2014

DOI: 10.1039/c3ta15114j

www.rsc.org/MaterialsA

In this paper, we demonstrate a series of metal-free and inexpensive TiO_2/carbon dot (CD) nanocomposites *via* facile hydrothermal synthesis from bidentate complexes of a green carbon source, vitamin C (VC). Other than the importance of deriving CDs from alternate carbon materials instead of graphitic precursors, the *in situ* transformed CDs from VC ensure the formation of chemically coupled heterostructures, TiO_2/CDs, which serve as efficient photocatalysts exhibiting a higher H_2 evolution rate from photocatalytic reactions up to 9.7 times than that of bare TiO_2. Interestingly, the H_2 evolution rate can effectively be tuned by VC amounts, hydrothermal temperatures and reaction durations. The mechanism of the enhanced H_2 evolution rate was also discussed, in which the synergetic effects of the hydrothermal treatment along with the favourable electron transfer ability and upconverted photoluminescence of CDs contribute to the improved photocatalytic behaviour.

1. Introduction

The conversion of solar energy into hydrogen, a potential candidate for clean and sustainable fuels of the future, offers an attractive and effective way to solve the increasingly urgent energy crisis and environmental pollution.[1–3] Given its high photoactivity and chemical inertness, TiO_2 has been extensively adopted as an efficient photocatalyst for water splitting, ever since its first utilization on photoelectrochemical (PEC) electrodes.[4] The poor light absorption and rapid electron/hole (e^-/h^+) recombination, however, greatly restrict the efficiency of TiO_2 photocatalytic behaviors.[5] Thus, the facile design of TiO_2 into heterostructured nanocomposites has been developed to improve its light harvesting and also to facilitate the e^-/h^+ separation,[6,7] for instance, doping with noble metals, such as Au,[8] or Pt,[9] combined with semiconductor quantum dots (QDs), like CdSe,[10] or sensitized by organic dyes, *e.g.* ruthenium bipyridyl derivatives.[11] In this respect, integrating TiO_2 with inexpensive and green materials in a simple way is highly desired for practical importance.

Carbon dots (CDs), a novel and eco-friendly zero-dimensional carbon nanomaterial, were discovered to boost the photocatalytic processes for plenty of photocatalysts, by virtue of their favourable upconverted photoluminescence (UCPL) feature and electron transfer ability.[12,13] Lee *et al.* first proved the availability of TiO_2/CD and SiO_2/CD hybrids for efficient photo-degradation of methyl blue.[14] Afterwards, CDs have been blended with Fe_2O_3,[15] Ag_3PO_4,[16] Cu_2O,[17] ZnO,[18] hematite[19] and CdS QDs[20] for the degradation of dyes and toxic gases, or even CO_2 conversion.[21] Recently, Kang *et al.* have confirmed that the graphite-derived CDs can be used for photoelectrochemical hydrogen generation,[22] indicating that CDs are promising candidates for photocatalytic water splitting. Nevertheless, the synthetic routes of CDs for photocatalytic purposes until now have been usually electrochemical exfoliation of graphite or ultrasonic preparation from graphene, which suffer the disadvantages of complex procedures, harsh post-treatments or low yields. Moreover, there is a concern of the CD-based photocatalysts, mostly of those that are physically loaded without chemical coupling, failing to generate stable interfaces between CDs and the host catalysts. Undoubtedly, the lack of interfacial bonding between the heterojunctions, despite rare studies, should not favor the migration of photo-induced electrons, thereby giving rise to an impoverished photocatalytic activity.[23–25] Hence, the pursuit of an easy and alternate method for synthesis of effective CDs, along with CD-incorporated nanocomposites with good interfaces *via* chemical reactions, is significant for improved photocatalytic behaviours.

Herein, we present a series of well-interfaced TiO_2/CD nanocomposites from bidentate complexes of TiO_2 nanoparticles and nanowires with vitamin C (VC) by simple hydrothermal synthesis. Owing to the reaction between titanium ions and *ortho*-substituted hydroxyl groups, VC can be favourably anchored at the TiO_2 surfaces. As a result, the *in situ* transformed CDs from VC are firmly attached to TiO_2 in the ultimate chemically coupled heterostructures, forming benign interfaces between the two components. The versatile TiO_2/CD nanocomposites in the ensembles of

Department of Electrical and Computer Engineering, National University of Singapore, 4 Engineering Drive 3, 117576, Singapore. E-mail: elehgw@nus.edu.sg

† Electronic supplementary information (ESI) available. See DOI: 10.1039/c3ta15114j

nanoparticles (NPs) and nanowires (NWs), even without the assistance of any metal ions, can enhance the solar H_2 evolution rate from photocatalytic water splitting. Moreover, the H_2 generation rate can be manipulated by VC amounts, hydrothermal temperatures and reaction durations. We consider that the introduction of CDs with unique properties onto TiO_2 surfaces should be responsible for the improved photocatalytic water splitting. This easy and economical method may pave an alternative way for the fabrication of green, low-cost, scalable and high-performance photocatalysts.

2. Experimental

2.1 Materials

Vitamin C (VC, also known as L-ascorbic acid) was purchased from Aldrich, and P25 powder (with an average particle diameter of ~21 nm) from Degussa. Methanol, ethanol, sodium hydroxide and hydrochloric acid were purchased from standard sources. All the chemicals were used as received without further purification.

2.2 Preparation of pure CDs

1 mg VC was dissolved in a mixture of 15 mL deionized water and 15 mL anhydrous ethanol, and stirred vigorously for 30 min. The as-formed transparent solution was then transferred into a 50 mL Teflon-lined stainless-steel autoclave and maintained at 90 °C for 4 h. After cooling to room temperature, a light yellow solution was obtained. The solution was centrifuged at 10 000 rpm for 30 min, and the supernatant was collected and filtered with an ultra-filtration membrane (0.2 μm) to remove the impurities and larger particles. The filtrate, *i.e.* the CD solution, was collected for further characterization.

2.3 Preparation of TiO_2 nanowires (NWs)

The TiO_2 NWs were prepared by the hydrothermal method as reported.[26] Typically, 1 g P25 powder was mixed with 25 mL NaOH solution (10 M) for 30 min to form a white suspension, which was then transferred into a 50 mL Teflon-lined stainless-steel autoclave and maintained at 150 °C for 24 h. The product was first washed with HCl solution (1 M) until pH = 1, and then with deionized water several times until pH = 5. After centrifugation, the white precipitate was collected and dried at 55 °C. The as-obtained white powder was further calcined at 400 °C for 2 h under ambient conditions, and the final product is noted as TiO_2 NWs.

2.4 Preparation of TiO_2 nanoparticle (NP)/CD nanocomposites

0.3 g P25 powder was first dispersed in a mixture of 15 mL deionized water and 15 mL anhydrous ethanol, and stirred vigorously for 30 min. Different amounts of VC (1.1, 0.1, 0.01, and 0.001 g) were then added into the above suspension and stirred for 30 min, which was transferred into a 50 mL Teflon-lined stainless-steel autoclave and maintained at 90, 150 and 200 °C for 2, 4 and 6 h, respectively. After cooling to room temperature, the product was centrifuged at 10 000 rpm for 30 min. The precipitate was collected, washed with deionized water and dried at 55 °C, which is noted as TiO_2 NP/CD nanocomposites, for further use.

2.5 Preparation of TiO_2 NW/CD nanocomposites

0.1 g ground TiO_2 NWs were dispersed in 10 mL deionized water and stirred vigorously for 30 min. 15 mL aqueous solution of VC (0.01 wt%) was then added into the suspension and stirred for 30 min to form NW/VC precursors. The mixed suspension was transferred into a 50 mL Teflon-lined stainless-steel autoclave and maintained at 90 °C for 4 h. The following procedures are similar to the case of NP/CD composites. The final product is noted as TiO_2 NW/CD nanocomposites, for further use.

2.6 Photocatalytic water splitting

5 mg TiO_2/CD nanocomposites, 9 mL DI water and 1 mL methanol were mixed in a quartz vial and stirred for 30 min to form a homogeneous suspension. Prior to photocatalytic water splitting, the suspension was purged with argon gas for 10 min. The measurements of H_2 evolution were carried out by magnetic stirring under illumination of a 300 W Xe lamp, and the readings were taken every 30 min within 2 h.

2.7 Photocurrent test of PEC cells

The PECs were realized by coating a layer of glycol suspensions of pure TiO_2 and TiO_2/CD nanocomposites on a FTO glass (1.5 × 2 cm) and dried at 55 °C. With the samples as working electrodes and Pt as the reference electrode, the amperometric *I–t* curves were recorded under an illumination of 300 mW cm^{-2} for three 30 s light-on–off cycles.

2.8 Characterization

Fourier transform infrared (FT-IR) spectra of TiO_2 and TiO_2/CD nanocomposites powder were recorded on a Shimadzu IRPrestige-21 FT-IR spectrophotometer, with 32 scans from 4000 to 500 cm^{-1} at a resolution of 4 cm^{-1}. High-resolution transmission electron microscopy (HRTEM) images of the CDs and TiO_2/CD nanocomposite solutions (1 wt%) were taken on a Philips CM300 transmission electron microscope. X-ray diffraction (XRD) spectra of the powder samples were recorded using a Philips X-ray diffractometer with Cu Kα radiation (λ = 1.541 Å). Thermogravimetric (TG) curves of the powders were collected on a SDT Q600 V8.3 Build 101 at 20 °C min^{-1} under air. UV-vis absorption spectra were obtained on a Shimadzu UV-3600 UV-vis spectrophotometer. Photoluminescence (PL) spectra and the two-dimensional (2D) PL distribution maps were measured on a Shimadzu RF-5301PC spectrofluorophotometer equipped with extra "specget" software under ambient conditions. H_2 uptake was measured using pressure composition isotherm measurements on a Shimadzu GC-2014AT gas chromatographer.

3. Results and discussion

Fig. 1 schematically depicts the generation of TiO_2/CD nanocomposites. Degussa P25, composed of *ca.* 80% anatase and 20% rutile TiO_2, was used as the source of TiO_2 NPs, and also as

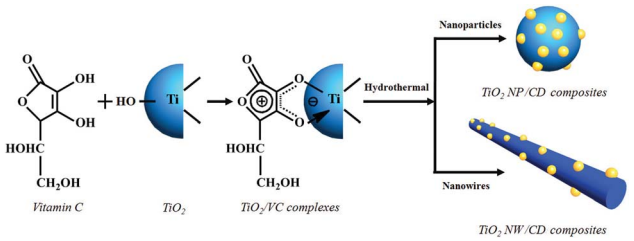

Fig. 1 Schematic illustration of the *in situ* hydrothermal synthesis of TiO_2/CD nanocomposites.

the precursor of TiO_2 NWs. The morphologies of TiO_2 1D structures are reported to rely on the size and crystalline phases of the TiO_2 sources,[27] in which commercially available P25 as the starting material should be conducive to the property control of the final NWs. VC, an essential nutrient for mankind, was chosen as the green precursor for CDs. When VC was added under ambient conditions, the TiO_2 suspension instantly turned from white to yellow or coffee colour depending on the VC amount (NPs) and light yellow (NWs), implying the yield of TiO_2/VC complexes from the reaction of hydroxyl groups in VC with titanium ions. After hydrothermal treatment, the immobilized VC was *in situ* transformed into CDs at the TiO_2 surfaces, producing the TiO_2/CD nanocomposites.

The morphologies, chemical compositions and optical properties of pure CDs are explored. As displayed in the high resolution transmission electron microscopy (HRTEM) images (Fig. 2a and b), these CDs have a relatively uniform particle distribution, and the average diameter (D_{ave}) is 4.7 nm. Moreover, an obvious crystalline structure is observed, with an interplanar spacing of 0.344 nm. These VC-derived CDs are rendered with some functional groups at their surfaces (FT-IR spectrum in Fig. 2c), including C=C (1617 cm^{-1}), C=O (1702 cm^{-1}), C–O (1019 and 750 cm^{-1}) and –OH (3363 cm^{-1}) groups.[28] These manifest the successful preparation of CDs from the hydrothermal treatment of VC. Typically, the CDs exhibit a UV absorption peak at *ca.* 250 nm and a PL emission peak at *ca.* 430 nm (Fig. 2d). Interestingly, the UCPL properties of the CDs are seen from their 2D PL distribution maps, wherein the PL emissions predominantly range from 340–390 nm upon the excitation of 300–380 nm (shorter wavelengths) and 500–690 nm (longer wavelengths), respectively (Fig. S1†).

As reported, VC can bind with TiO_2 due to the reaction between titanium ions and the *ortho*-substituted hydroxyl groups of the furan ring, ultimately creating a bidentate complex.[29] Fig. 3 shows the typical expansion of Ti 2p, C 1s and O 1s peaks for the X-ray photoelectron spectroscopy (XPS) spectra of the as-formed TiO_2 NPs/VC complex, respectively (VC : TiO_2 = 1 : 300, w/w). The presence of Ti $2p_{3/2}$ at 459.1 eV and Ti $2p_{1/2}$ at 464.8 eV indicates a slight energy shift compared to bare TiO_2,[30,31] which probably arises from the coupling of TiO_2 with VC. The C=O (289.0 eV), C–O (286.5 eV) and C–C/C=C (285.1 eV) groups along with the Ti–O group (530.5 eV) are also detected, whereas the peak ascribed to Ti–C bonds at ~281 eV is not observed. Hereby, clear evidence is provided for the chemically coupled TiO_2/VC complex through the Ti–O–C bond.

TiO_2/CD nanocomposites were achieved from TiO_2/VC bidentate complexes by hydrothermal synthesis at certain temperatures for different durations. Thermogravimetric (TG) curves of TiO_2 NPs and NP/CD nanocomposites (to observe clearly, the weight ratio of VC to TiO_2 1 : 60 is used) were recorded to calculate the weight ratio of carbon in the composites (Fig. S2†). The 0.85% weight loss of both NPs and composites before 200 °C should be attributed to the elimination of adsorbed water. The 0.58% weight loss observed between 200 and 400 °C in the NPs may result from the dehydroxylation of surface-attached water and –OH groups (black line),[32] while the weight loss drops by 1.35% in the composites (red line), indicating the decomposition process of carbon. Therefore, the carbon content accounts for *ca.* 0.77 wt% in the composites.

Fig. 4 shows the HRTEM images of pure TiO_2 and the TiO_2/CD composites originated from the as-obtained complexes at

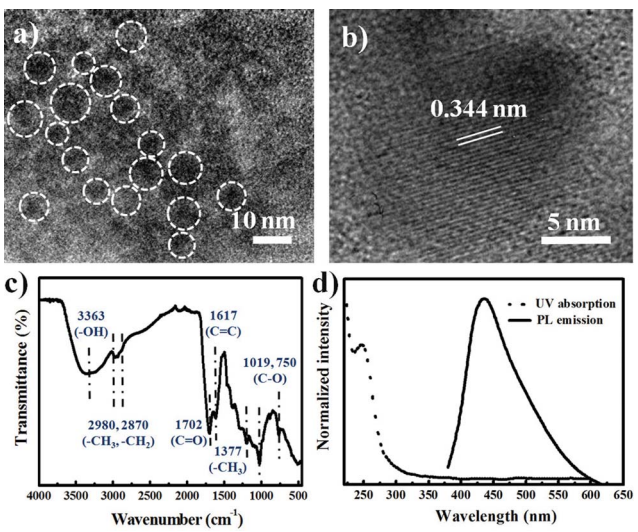

Fig. 2 (a and b) HRTEM images, (c) FT-IR spectrum and (d) UV-vis absorption and PL emission spectra of pure VC-derived CDs.

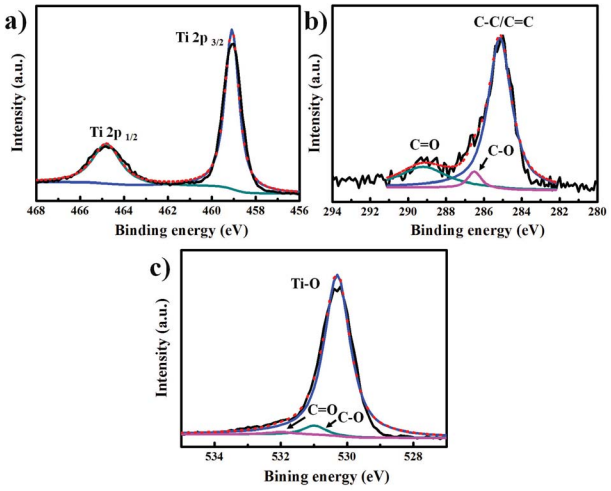

Fig. 3 (a) Ti 2p, (b) C 1s and (c) O 1s XPS spectra of the TiO_2 NP/VC complex (VC : TiO_2 = 1 : 300, w/w).

90 °C for 4 h. Fig. 4a–c (TiO_2 NPs) reveal two interplanar spacings of 0.355 and 0.328 nm in the well-resolved lattice fringes, indicating anatase and rutile phases in the TiO_2 nanoparticles, respectively.[33] It is clearly seen from Fig. 4d that an individual carbon dot, with a distinguished interplanar spacing of 0.342 nm, is closely attached onto an anatase TiO_2 nanoparticle surface. X-ray diffraction (XRD) patterns of bare TiO_2 NPs and NP/CD nanocomposites were also collected (Fig. S3†). Several strong and sharp diffraction peaks are observed in TiO_2 NPs, which can be indexed to anatase (JCPDS card 01-084-1285) and rutile (JCPDS card 00-034-0180) phases,[34] corresponding to the TEM images. The peaks remain almost unchanged in the NP/CD composites, but the peak at ~26° ascribed to carbon is too weak to be observed, which is due to the tiny amount of CDs in the composites, similar to the cases reported by Kang's[16] and Cui's groups.[35] Moreover, a large quantity of TiO_2 NWs with a uniform diameter distribution of ~15 nm can be clearly observed, which are hundreds of nanometers in length (Fig. S4†). The HRTEM image (Fig. 4e) of a single TiO_2 nanowire shows an interspacing of 0.354 nm, indicating that anatase TiO_2 dominates in the NWs, which is further identified by its XRD patterns (Fig. S5†). From the HRTEM image of TiO_2 NW/CD nanocomposites (Fig. 4f), several carbon dots (red circle area; the interplanar spacing is 0.342 nm) can be observed to be adhered to the surfaces of the TiO_2 NWs. The intimate interfaces between TiO_2 and CDs should control the physicochemical characteristics of the nanocomposites, which may benefit the charge transport between the two components.

The as-synthesized nanocomposites were utilized for hydrogen production from photocatalytic water splitting. In this case, we found that the H_2 evolution rate can be optimized by tuning the VC amount, hydrothermal temperatures and reaction durations. Fig. 5a shows the time course of H_2 generation of the TiO_2 NPs and NP/CD nanocomposites obtained from different VC amounts (90 °C, 4 h). The attained H_2 evolution rate shows a linear relationship with the illumination time, denoting a continuous and steady water splitting process. Pure TiO_2 NPs were able to generate H_2 at a rate of 76.5 μmol g^{-1} h^{-1} (black line), while no H_2 was acquired in the cases of 1.1 and 0.1 g VC amounts (the red and yellow lines are overlapped). FT-IR spectra of the TiO_2 NP/VC complexes at different VC amounts along with bare TiO_2 NPs and VC were collected (Fig. S6†). The peaks at 1636 and 1384 cm^{-1} were assigned to the in-phase bending vibration of –OH groups of TiO_2. When the VC amount is 1.1 g, the FT-IR spectrum of the corresponding complex is identical to pure VC, indicating that the amount of VC supersedes that of TiO_2. Similarly, the VC amount is also considered as excessive on the TiO_2 surface when it is 0.1 g. Accordingly, the TiO_2 particles are completely surrounded by CDs after hydrothermal treatment (TEM images shown in Fig. S7†), which may hinder the light irradiation to TiO_2 particles and then lead to the "poisoning" of the host catalyst.[36] As for the 0.01 g case, the nanocomposites can produce hydrogen at a slower rate of 48.6 μmol g^{-1} h^{-1} (blue line), which might be ascribed to partial wrapping of CDs on the TiO_2 particles. The nanocomposites, when the VC amount was as low as 0.001 g, reached the highest H_2 evolution rate of 361.9 μmol g^{-1} h^{-1} (green line), which is 4.7 times higher than that of bare TiO_2. Under this optimal condition, the CDs should be favourably distributed on the TiO_2 surfaces for the best light absorption of TiO_2. The NP/CD nanocomposites for water splitting were carried out for another two cycles, with the H_2 evolution rate slightly improved (Fig. 5b), suggesting that the nanocomposites are capable for long-term runs.

The H_2 generation rates of NP/CD nanocomposites synthesized at different hydrothermal temperatures (90, 150 and 200 °C) and reaction times (2, 4 and 6 h) were also studied (Fig. 6; the VC

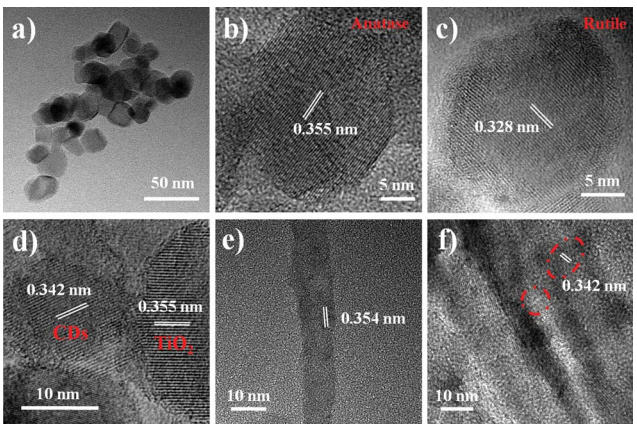

Fig. 4 HRTEM images of (a–c) TiO_2 NPs, (d) TiO_2 NP/CD nanocomposites, (e) TiO_2 NWs and (f) TiO_2 NW/CD nanocomposites.

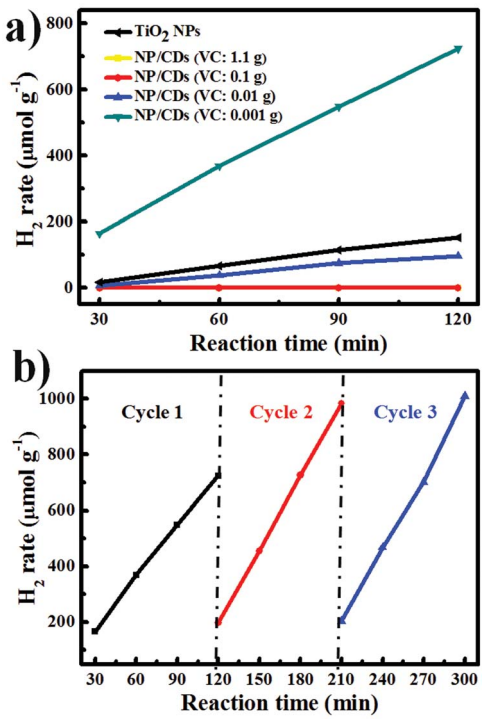

Fig. 5 (a) Time course of H_2 production from TiO_2 NPs and NP/CD composites synthesized at different VC amounts: 1.1, 0.1, 0.01 and 0.001 g. (b) A typical time course of H_2 production from NP/CD composites for 3 cycles.

amount is 0.001 g). The samples are named after their reaction temperatures and durations, *e.g.* 90-2. Compared to bare TiO_2 NPs, the H_2 generation rates of all these nanocomposites were enhanced. In general, the H_2 generation rate gradually increased with the hydrothermal time for the 90 and 150 °C samples, with the highest rates reaching 375.8 and 454.3 μmol g^{-1} h^{-1}, respectively. In contrast, the H_2 rates of 200 °C nanocomposites seem to decline with the reaction durations, but the highest H_2 generation rate reached 739.0 μmol g^{-1} h^{-1} for 200-2 which is 9.7 times higher than TiO_2. The difference in the H_2 generation rates for various samples might be related to the UCPL properties of the CDs (see Fig. S1†). First, extending the hydrothermal durations at lower temperatures (*i.e.* 90 and 150 °C) displays unshifted but broader PL emissions of the nanocomposites, leading to gradually better H_2 production behaviour. Second, the PL emissions centre in the vicinity of 385 nm under ideal conditions (200 °C, 2 h), with the PL intensities appropriate for the synergistic effects of CDs and TiO_2 NPs (the irradiation wavelength to induce its best photocatalytic behaviour is 380 nm) to give the highest H_2 rate. However, prolonging the reaction time to 6 h at 200 °C caused the red-shift of PL emissions to ~420 nm, thus resulting in a slower H_2 generation rate.

The *in situ* chemical bonded CD-based 0D nanocomposites turn out to be effective for enhanced photocatalytic hydrogen production. Subsequently, 1D TiO_2 NW/CD nanocomposites were fabricated and employed for water splitting. Fig. 7 displays the H_2 generation rate of bare TiO_2 NWs (black line) and TiO_2 NW/CD nanocomposites from hydrothermal synthesis at 90 °C for different hours. The H_2 generation rate of bare NWs is 286.4 μmol g^{-1} h^{-1}, and is improved to 302.6, 1189.7 and 604.7 μmol g^{-1} h^{-1} for the NW/CD nanocomposites obtained at 2, 4 and 6 h, respectively. Similar to that of NP/CD nanocomposites, the PL emissions of all the NW/CD nanocomposites centre at ~390 nm, among which the 4 h sample, with the highest H_2 generation rate, shows the broadest PL emission range (Fig. S8†). This illustrates that this *in situ* coupling of CDs is structurally versatile.

To understand the mechanism of the enhanced H_2 generation rate, the photoresponses of TiO_2 and TiO_2/CD nanocomposites over time were conducted (Fig. 8). The two-electrode

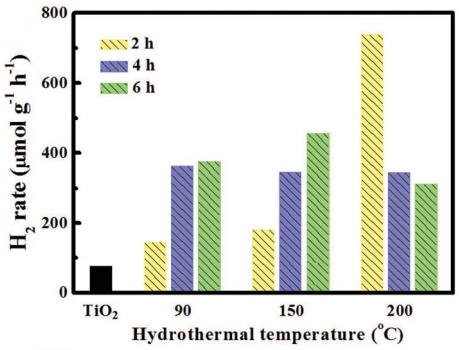

Fig. 6 Photocatalytic H_2 production studies of TiO_2 NPs and NP/CD composites synthesized at different hydrothermal temperatures (90, 150 and 200 °C) and times (2, 4 and 6 h).

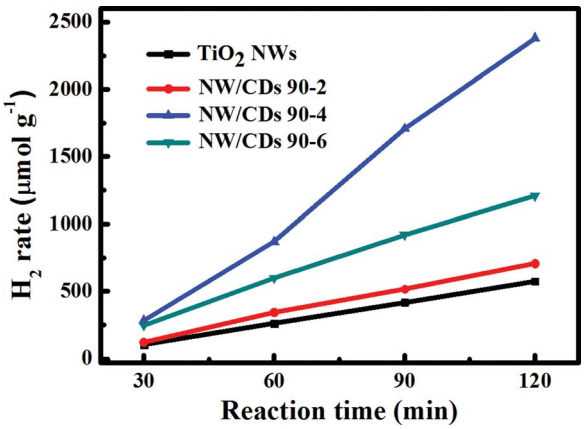

Fig. 7 Time course of H_2 production from TiO_2 NWs and NW/CD nanocomposites synthesized at 90 °C for 2, 4 and 6 h.

PEC cells are based on the working electrodes of pure TiO_2 and TiO_2/CD nanocomposites, with their amperometric *I–t* curves acquired at three light on–off cycles within 30 s. The photocurrent of TiO_2 NPs peaked at *ca.* 0.04 μA cm^{-2} and then decayed to a steady state of *ca.* 0.01 μA cm^{-2} after ~15 s. Whereas, the initial photocurrent of the NP/CD nanocomposites reached as high as *ca.* 0.11 μA cm^{-2} and eventually approached to a plateau at *ca.* 0.03 μA cm^{-2}, which is ~3 times higher than that of bare TiO_2 NPs. The photocurrent responses in the case of NWs are similar, with a steady photocurrent of 0.08 μA cm^{-2} for pure NWs, and as high as ~0.24 μA cm^{-2} for NW/CD nanocomposites. The 2.6-fold higher photocurrent of NWs over NPs indicates better electron transport along the unique 1D nanowire than 0D nanoparticles. Along with more photocatalytic reaction sites than NPs, NWs show nearly a

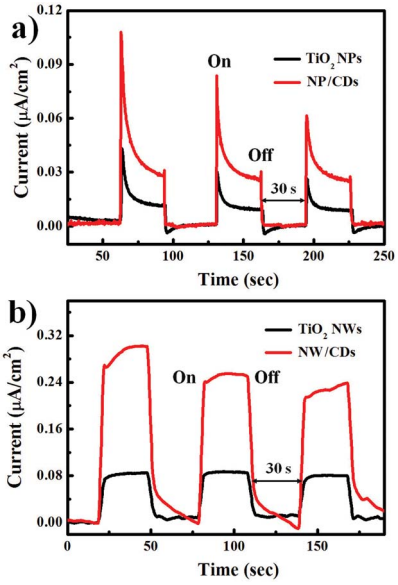

Fig. 8 Photocurrent responses of the PEC cells using (a) TiO_2 NPs and NP/CD composites and (b) TiO_2 NWs and NW/CD composites as working electrodes for three 30 s light-on–off cycles (hydrothermal temperature: 90 °C and hydrothermal durations: 4 h).

4 times higher H_2 generation rate than NPs, as shown above.[37] The higher photocurrent density in TiO_2/CD composites suggests more effective separation of the e^-/h^+ at the interfaces, which is beneficial for the enhanced H_2 generation rate.[38,39]

Finally, a tentative discussion on the enhanced hydrogen generation rate is given below. Firstly, the hydrothermal treatment is able to bestow higher photoactivity on TiO_2, which should result from increased hydroxyl groups on its surface to mediate the charge transfer.[40] The photocatalytic H_2 production of hydrothermally treated TiO_2 NPs (NP-HT, 90 °C for 2 and 4 h) was performed strictly under the same conditions. The H_2 generation rates of both TiO_2-HTs are nearly two times higher than untreated TiO_2 NPs (Fig. S9†), confirming that the hydrothermal treatment contributes partly to the enhanced water splitting behaviour. Secondly, the superior interfacing of CDs with TiO_2 should benefit the electron transfer behaviour during the photocatalytic process. For comparison, the mixture of CDs and TiO_2 NPs by merely physical blending shows a feeble H_2 evolution rate (Fig. S10†), which is likely due to the unfavourable interfacial coupling of CDs and TiO_2 during the vigorous stirring of the water splitting process. Indeed, CDs are able to serve as electron acceptors and donors,[41] wherein the photo-induced electrons can transfer from CDs to TiO_2 surfaces, and then the redundant electrons on TiO_2 can transfer back to the CD particles, as illustrated in Fig. 9. Thirdly, the absorption edges of the TiO_2 red-shifted after bonding with CDs (Fig. 10), indicating that the TiO_2/CD composites have an extended solar absorption spectrum and can absorb more light during the photocatalytic process (Fig. 9). The H_2 generation rates of the composites are found to correspond well with the absorption edges. For instance, the absorption edge of 200-2 NP/CD composites (with the highest H_2 evolution rate) extends to as far as *ca.* 480 nm. Finally, CDs possess fascinating UCPL properties that can be employed for efficient photocatalysis. The 2D PL maps of typical NP/CD nanocomposites (selectively the highly performed NPs/CDs 90-6, 150-6 and 200-2) reveal obvious UCPL properties, with the PL emissions ranging from 350 to 440 nm but centering at 380 nm upon the excitation wavelength of 530–690 nm (Fig. 10, inset: in the index, red colour indicates higher intensity while blue indicates lower intensity). The extension of light absorption to a longer wavelength, together with the PL conversion from a longer wavelength to a shorter wavelength, should induce better light harvesting of TiO_2 for an enhanced H_2 generation rate.

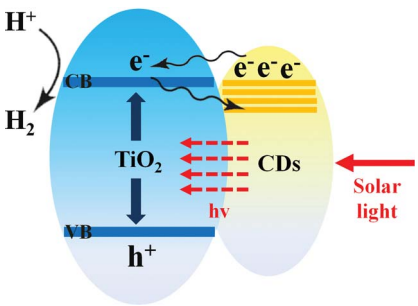

Fig. 9 Schematic illustration for the mechanism of the enhanced hydrogen generation in TiO_2/CD nanocomposites.

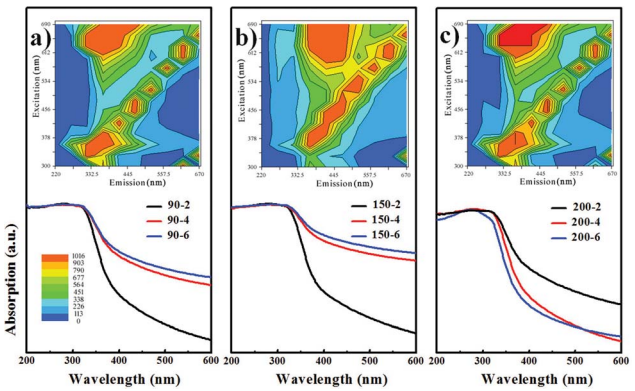

Fig. 10 UV-vis absorption spectra of NP/CD nanocomposites obtained under different conditions. The inset shows the PL distribution maps of NP/CD nanocomposites of (a) 90-6, (b) 150-6 and (c) 200-2.

4. Conclusions

In conclusion, a series of novel metal-free TiO_2/CD composites have been *in situ* synthesized from bidentate TiO_2/VC complexes by the hydrothermal method. The effects of VC amounts, hydrothermal temperatures and times have been explored for H_2 generation from photocatalytic water splitting. The NP/CD nanocomposites obtained at 200 °C for 2 h with a VC amount of 0.001 g show a 9.7-fold higher H_2 production rate than bare TiO_2 NPs. The NW/CD nanocomposites prepared at 90 °C for 4 h also produce hydrogen at a rate of 1189.7 μmol g^{-1} h^{-1}, which is 4.2 times higher than that of bare TiO_2 NWs. This facile and green access to versatile nanocomposite photocatalysts may offer valuable opportunities for the synthesis of effective heterostructures for photocatalysis.

Acknowledgements

This work is supported by the National University of Singapore (NUS) grant R-263-000-653-731/654-112 and R-263-000-A96-305.

Notes and references

1 X. Chen, S. Shen, L. Guo and S. S. Mao, *Chem. Rev.*, 2010, **110**, 6503–6570.
2 K. Maeda and K. Domen, *J. Phys. Chem. Lett.*, 2010, **1**, 2655–2661.
3 F. E. Osterloh, *Chem. Soc. Rev.*, 2013, **42**, 2294–2320.
4 A. Fujishima and K. Honda, *Nature*, 1972, **238**, 37–38.
5 R. Daghrir, P. Drogui and D. Robert, *Ind. Eng. Chem. Res.*, 2013, **52**, 3581–3599.
6 A. Kudo and Y. Miseki, *Chem. Soc. Rev.*, 2009, **38**, 253–278.
7 H. Tong, S. Ouyang, Y. Bi, N. Umezawa, M. Oshikiri and J. Ye, *Adv. Mater.*, 2012, **24**, 229–251.

8 P. A. DeSario, J. J. Pietron, D. E. DeVantier, T. H. Brintlinger, R. M. Stroud and D. R. Rolison, *Nanoscale*, 2013, **5**, 8073–8083.
9 O. Rosseler, M. V. Shankar, M. K.-L. Du, L. Schmidlin, N. Keller and V. Keller, *J. Catal.*, 2010, **269**, 179–190.
10 Y.-L. Lee, C.-F. Chi and S.-Y. Liau, *Chem. Mater.*, 2010, **22**, 922–927.
11 Y. Park, S.-H. Lee, S. O. Kang and W. Choi, *Chem. Commun.*, 2010, **46**, 2477–2479.
12 S. Zhuo, M. Shao and S.-T. Lee, *ACS Nano*, 2012, **6**, 1059–1064.
13 H. Li, Z. Kang, Y. Liu and S.-T. Lee, *J. Mater. Chem.*, 2012, **22**, 24230–24253.
14 H. Li, X. He, Z. Kang, H. Huang, Y. Liu, J. Liu, S. Lian, C. H. A. Tsang, X. Yang and S.-T. Lee, *Angew. Chem.*, 2010, **122**, 4532–4536.
15 H. Zhang, H. Ming, S. Lian, H. Huang, H. Li, L. Zhang, Y. Liu, Z. Kang and S.-T. Lee, *Dalton Trans.*, 2011, **40**, 10822–10825.
16 H. Zhang, H. Huang, H. Ming, H. Li, L. Zhang, Y. Liu and Z. Kang, *J. Mater. Chem.*, 2012, **22**, 10501–10506.
17 H. Li, R. Liu, Y. Liu, H. Huang, H. Yu, H. Ming, S. Lian, S.-T. Lee and Z. Kang, *J. Mater. Chem.*, 2012, **22**, 17470–17475.
18 H. Yu, H. Zhang, H. Huang, Y. Liu, H. Li, H. Ming and Z. Kang, *New J. Chem.*, 2012, **36**, 1031–1035.
19 B. Y. Yu and S.-Y. Kwak, *J. Mater. Chem.*, 2012, **22**, 8345–8353.
20 Y. Liu, Y.-X. Yu and W.-D. Zhang, *J. Alloys Compd.*, 2013, **569**, 102–110.
21 L. Cao, S. Sahu, P. Anilkumar, C. E. Bunker, J. Xu, K. A. S. Fernando, P. Wang, E. A. Guliants, K. N. Tackett and Y.-P. Sun, *J. Am. Chem. Soc.*, 2011, **133**, 4754–4757.
22 X. Zhang, F. Wang, H. Huang, H. Li, X. Han, Y. Liu and Z. Kang, *Nanoscale*, 2013, **5**, 2274–2278.
23 Y. T. Liang, B. K. Vijayan, O. Lyandres, K. A. Gray and M. C. Hersam, *J. Phys. Chem. Lett.*, 2012, **3**, 1760–1765.
24 P. W. King, *Biochim. Biophys. Acta, Bioenerg.*, 2013, **1827**, 949–957.
25 L.-W. Zhang, H.-B. Fu and Y.-F. Zhu, *Adv. Funct. Mater.*, 2008, **18**, 2180–2189.
26 W. Wang, H. Lin, J. Li and N. Wang, *J. Am. Ceram. Soc.*, 2008, **91**, 628–631.
27 C.-C. Tsai and H. Teng, *Chem. Mater.*, 2004, **16**, 4352–4358.
28 B. Zhang, C. Liu and Y. Liu, *Eur. J. Inorg. Chem.*, 2010, **2010**, 4411–4414.
29 Y. Ou, J.-D. Lin, H.-M. Zou and D.-W. Liao, *J. Mol. Catal. A: Chem.*, 2005, **241**, 59–64.
30 M. Xing, J. Zhang, F. Chen and B. Tian, *Chem. Commun.*, 2011, **47**, 4947–4949.
31 M. Gao, C. K. N. Peh, W. L. Ong and G. W. Ho, *RSC Adv.*, 2013, **3**, 13169–13177.
32 M. M. Oliveira, D. C. Schnitzler and A. J. G. Zarbin, *Chem. Mater.*, 2003, **15**, 1903–1909.
33 Q. Xu, Y. Ma, J. Zhang, X. Wang, Z. Feng and C. Li, *J. Catal.*, 2011, **278**, 329–335.
34 W. Liu, D. Chen, S. H. Yoo and S. O. Cho, *Nanotechnology*, 2013, **24**, 405706–405713.
35 M. Sun, X. Ma, X. Chen, Y. Sun, X. Cui and Y. Lin, *RSC Adv.*, 2014, **4**, 1120–1127.
36 Y. Zhang, Z.-R. Tang, X. Fu and Y.-J. Xu, *ACS Nano*, 2010, **4**, 7303–7314.
37 J. Jitputti, Y. Suzuki and S. Yoshikawa, *Catal. Commun.*, 2008, **9**, 1265–1271.
38 Y. Gao, X. Ding, J. Liu, L. Wang, Z. Lu, L. Li and L. Sun, *J. Am. Chem. Soc.*, 2013, **135**, 4219–4222.
39 H. M. Chen, C. K. Chen, R.-S. Liu, L. Zhang, J. Zhang and D. P. Wilkinson, *Chem. Soc. Rev.*, 2012, **41**, 5654–5671.
40 J. Yu, H. Yu, B. Cheng, M. Zhou and X. Zhao, *J. Mol. Catal. A: Chem.*, 2006, **253**, 112–118.
41 X. Wang, L. Cao, F. Lu, M. J. Meziani, H. Li, G. Qi, B. Zhou, B. A. Harruff, F. Kermarrec and Y.-P. Sun, *Chem. Commun.*, 2009, 3774–3776.